

Electrodeposition of Co–Ni–P/graphene oxide composite coating with enhanced wear and corrosion resistance

Cansen Liu¹, Dongdong Wei¹, Xiaoye Huang¹, Yongjin Mai¹, Liuyan Zhang¹, Xiaohua Jie^{1,a)} 

¹School of Materials and Energy, Guangdong University of Technology, Guangzhou 510006, China

^{a)}Address all correspondence to this author. e-mail: cnxyyz3@gdut.edu.cn

Received: 14 November 2018; accepted: 4 January 2019

Coatings with low friction coefficient and excellent anti-wear and anticorrosion performances are of great interest for fundamental research and practical applications. In the present study, Cobalt–nickel–phosphorus/graphene oxide (Co–Ni–P/GO) composite coating is prepared by a pulse electrodeposition method. Effect of the embedded GO sheets on the microstructures, microhardness, and electrochemical and tribological behaviors of the Co–Ni–P/GO composite coating are researched in detail. The results reveal that the co-deposition of GO sheets significantly improves the microhardness of the as-prepared Co–Ni–P/GO composite coating and changes the morphology of the Co–Ni–P coating from hemispheric structure to nodule structure with smaller globular particles for the Co–Ni–P/GO composite coating. In addition, friction and wear tests show that the incorporation of GO sheets endows the Co–Ni–P/GO composite coating with remarkable friction reduction and improved wear resistance. Electrochemical corrosion tests demonstrate that the Co–Ni–P/GO composite coating possesses better corrosion resistance than the Co–Ni–P coating.

Introduction

The use of hard chromium (Cr) coating, with extensive applications in aerospace, automotive, marine, and electronics sectors, has been strictly regulated and restricted because of severe health and environmental problems caused by the hexavalent Cr in the electrolyte [1]. Ni–P and its composite coatings with high microhardness, good wear, and corrosion resistance were considered as a promising alternative material for the hard Cr coatings in critical engineering applications [2, 3]. Minimizing friction and wear is essential to improve the efficiency and service life of components, and tribological coatings with low coefficient of friction (COF) are sought-after in the modern industry. However, the COF of Ni–P coatings is in the range of 0.45–0.7 under dry lubrication against different counterface materials [4, 5]. Existing researches has demonstrated that the co-deposition of Co-rich Ni–Co alloy coatings showed friction reduction and anti-wear improvement [6]. The alloying of Co into Ni–P matrix is expected to reduce the COF and improve the tribological performance of the resulting coatings.

Co–Ni–P coatings are prepared by electroless plating and electrodeposition. In comparison with electroless plating, electrodeposition has advantages, such as simplicity and low

costs of plating process. Thickness, morphology, and phase structure of the coating are easy to be controlled by adjusting the electrical parameters [7, 8, 9, 10, 11]. Co–Ni–P coatings are normally applied as magnetic recording media [12], microwave absorptive materials [13], and electrocatalytic materials for water electrolysis [14]. Nevertheless, tribological and electrochemical performances of the Co–Ni–P coatings have not received much attention, although these properties are important for their industrial application under wear and corrosion conditions. Moreover, the demand for high-quality coatings becomes more rigorous with the industrial development and enhanced living conditions. Single-alloy coating cannot completely meet the requirement of the practical application conditions. Composite coatings, with alterable microstructure and capability by the intercalation of second-phase particles intercalate into the metal electrodeposit, have a highly interesting application in technologies and industries. Previous studies have confirmed that the incorporation of particle into metal matrix endowed the resulting composite coatings with enhanced anti-oxidant, anticorrosion, and friction properties [15, 16, 17, 18, 19, 20].

Graphene is expected to be an ideal enhancement of metal matrix composite coating for its superior mechanical,

electrochemical, thermal, and lubricating capacity [21]. Nevertheless, graphene is hard to be uniformly dispersed in the plating solution as there are no functional groups on its surface, limiting its potential application for the preparation of composite coatings. Graphene oxide (GO), the oxidized form of graphene, possesses remarkable properties and hydrophilic functional groups, such as $-OH$ and $-COOH$, which favor its uniform dispersion in the solution [22, 23, 24]. Thus, the co-deposition of Co–Ni–P/GO composite coating with excellent performances is feasible and expected. In fact, some researches has reported that GO, as a third-phase particle in electroplating, endowed the composite coatings with noble properties. Kumar et al. [25] showed that the Ni/graphene composite coatings electroplated on mild steel exhibited excellent corrosion resistance. Jiang et al. [26] fabricated Ni–Mo/GO composite coating on low-carbon steel by direct current electrodeposition with ultrasonic vibration and demonstrated that distribution of reduced GO endowed the composite coating with higher microhardness, enhanced oxidation resistance, and corrosion resistance. Xue et al. [27] prepared Ni–GO composite coatings by pulse electrodeposition technique under supercritical carbon dioxide and found that the introduction of reduced graphene oxide (RGO) into the composite coating significantly improved the wear resistance and friction reduction of the deposit.

In this study, Co–Ni–P/GO composite coatings were first obtained by an electroplating process. The effect of the incorporation of GO sheets on the microstructure, microhardness, and tribological and electrochemical performances of Co–Ni–P/GO composite coatings was systemically investigated. The introduction of GO sheets endows the Co–Ni–P/GO composite coatings with superior anti-wear and friction-reducing performances as well as better corrosion resistance property. The high-performance as-prepared composite coating is expected as a promising alternative material for the hard chromium coating in critical engineering applications.

Results

Microstructure and hardness

Scanning electron microscopic (SEM) images of the Co–Ni–P and Co–Ni–P/GO composite coatings surface are presented in Fig. 1. The Co–Ni–P coating shows a relative smooth surface of hemispheric structure with different diameter [Figs. 1(a) and 1(b)]. Cross-sectional view of the Co–Ni–P coating [Fig. 1(c)] shows a flat surface with a thickness about 20 μm . In contrast, the Co–Ni–P/GO composite coating surface displays a rough surface of nodule structure [Fig. 1(d)], which might result from the incorporation of GO sheets into Co–Ni–P matrix. Enlarged image of Fig. 1(e) reveals that the nodule structure is composed of smaller particles and GO sheets embedded in the Co–Ni–P matrix through the co-deposition process. The well-known carbon D

band and G band observed in the Raman spectra [inset image in Fig. 1(e)] indicate that GO sheets are co-deposited in composite coatings. The higher I_D/I_G intensity ratio (1.27) in Raman spectra with respect to that of original GO sheets (0.95) suggests that GO sheets in the resulting composite coating have been reduced [28]. Cross-sectional view of the Co–Ni–P/GO composite coating [Fig. 1(f)] shows an uneven surface, which is corresponding to the SEM image shown in Fig. 1(d).

Figure 2(a) shows the X-ray diffraction (XRD) patterns of the Co–Ni–P and Co–Ni–P/GO composite coatings. Both the Co–Ni–P and Co–Ni–P/GO composite coatings display a typical amorphous structure, as the broad peak centered at approximately 45° is clearly seen in Fig. 2(a), which is because of the high phosphorus content of the as-plated coatings. The result of Energy-dispersive X-ray spectroscopy (EDS) analysis shows that the phosphorus content of the Co–Ni–P and Co–Ni–P/GO composite coatings is both higher than 12 at% [Figs. 2(b) and 2(c)]. Sankara Narayanan et al. [29] suggested that the presence of phosphorus prevented the nucleation of nickel/cobalt phase and resulted in an amorphous structure.

Figure 3 presents the comparison of microhardness of the Co–Ni–P and Co–Ni–P/GO composite coatings. The microhardness of Co–Ni–P/GO composite coatings is about 600 HV, which increases by 33% compared with the Co–Ni–P coatings (450 HV). Because no obvious change in diffraction peaks is observed in Fig. 2(a), it can be deduced that the incorporation of GO sheets into the Co–Ni–P matrix is the main reason for the microhardness enhancement.

Wear and corrosion properties

Figure 4(a) gives the typical COF curves of the Co–Ni–P and Co–Ni–P/GO composite coatings. Both the COF curves of the as-deposited coatings climb to a certain value beyond a short run-in period and keep at that value until the end of the sliding. In addition, the COF of the Co–Ni–P/GO composite coating is more stable than that of Co–Ni–P coating with the increasing sliding distance, which indicates that the co-deposition of GO sheets into the Co–Ni–P matrix favors the formation of steady contact interface during the sliding process. Figure 4(b) presents the average COF and wear rates of the Co–Ni–P and Co–Ni–P/GO composite coatings. The Co–Ni–P/GO composite coatings display an average COF of 0.29, which is smaller than that of 0.38 for the Co–Ni–P coatings. The COF of the Co–Ni–P and Co–Ni–P/GO composite coatings are both smaller than the range of 0.45–0.7 for the Ni–P coating. These results demonstrate that the alloying of Co and insertion of GO sheets into Ni–P matrix endow the resulting coatings with friction-reducing property. Figure 4(b) also shows that the Co–Ni–P/GO composite coatings have an average wear rate of about $5.29 \times 10^{-6} \text{ mm}^3/(\text{N m})$, which is much lower than that

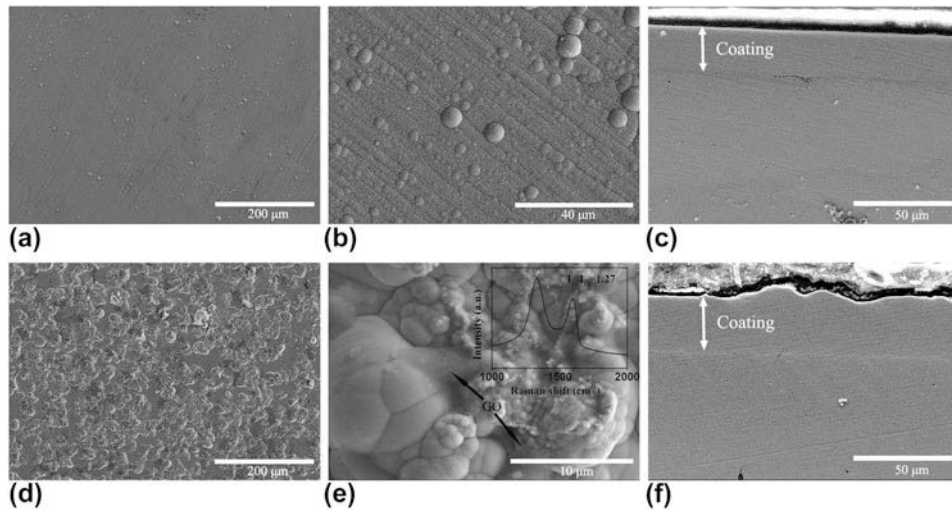


Figure 1: Surface and cross-sectional morphologies of the (a–c) Co–Ni–P and (d–f) Co–Ni–P/GO composite coatings. The inset in Fig. 1(e) is the Raman spectroscopy obtained from the Co–Ni–P/GO composite coating.

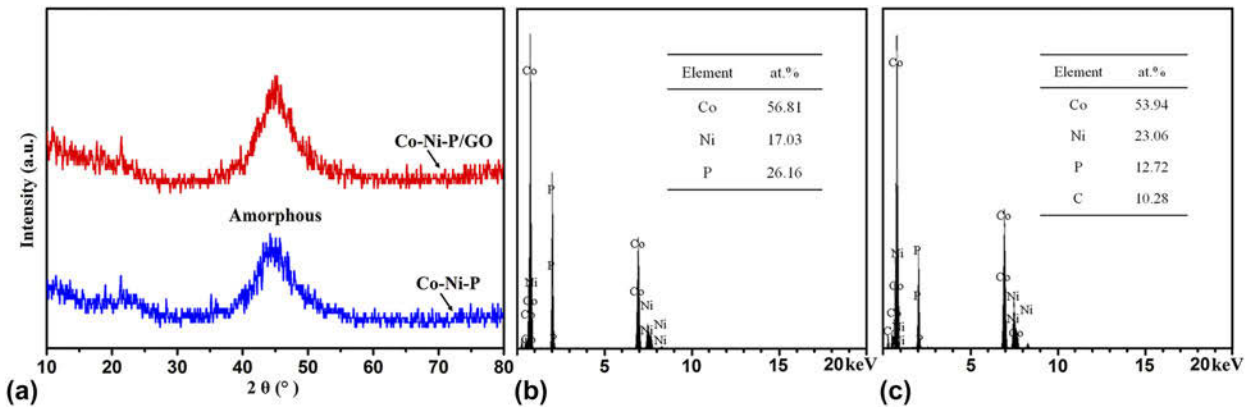


Figure 2: (a) XRD patterns of Co–Ni–P and composite coatings and EDX analysis of the (b) Co–Ni–P and (c) Co–Ni–P/GO composite coatings.

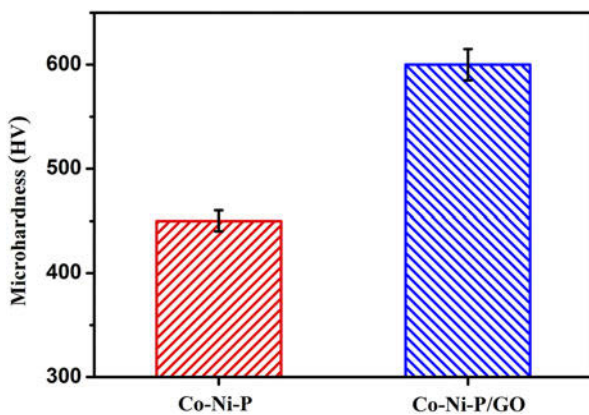


Figure 3: Microhardness of the Co–Ni–P and Co–Ni–P/GO composite coatings.

of $11.08 \times 10^{-6} \text{ mm}^3/(\text{N m})$ for the Co–Ni–P coatings, suggesting that the Co–Ni–P/GO composite coatings possess better tribological performance than the Co–Ni–P coatings.

Figure 5(a) shows the potentiodynamic polarization curves of the Co–Ni–P and Co–Ni–P/GO composite coatings evaluated in 3.5 wt% NaCl solution. Corrosion potential (E_{corr}), corrosion current density (i_{corr}), and corrosion rate that obtained from the potentiodynamic polarization curves are given in Table I. Co–Ni–P coating show an E_{corr} of -433.7 mV , and the Co–Ni–P/GO composite coating shifts to a more positive E_{corr} of -352.5 mV than the Co–Ni–P coating. Moreover, Co–Ni–P/GO composite coating displays a low i_{corr} value, which is about one fifth of the Co–Ni–P coating. Furthermore, the corrosion rate of the Co–Ni–P/GO composite coating is approximately 14% of the Co–Ni–P coating. These results reveal that the incorporation of GO sheets promotes the Co–Ni–P/GO composite coating with superior corrosion resistance than the Co–Ni–P coating according to its more positive E_{corr} , lower i_{corr} , and lower corrosion rate. Besides, the anticorrosion performance of the Co–Ni–P/GO composite coating is better than that of other reported GO-enhanced

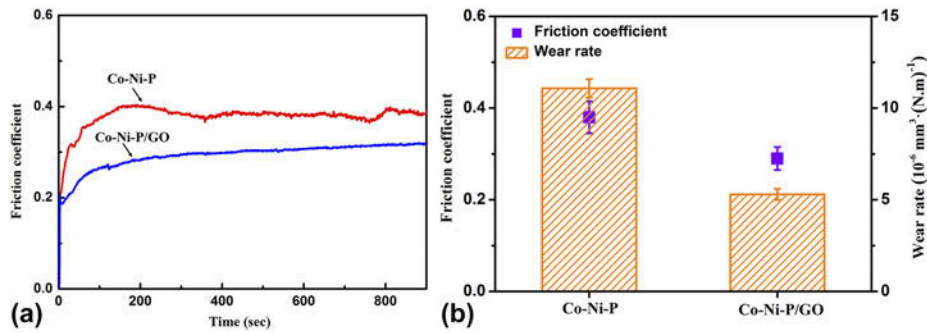


Figure 4: (a) Typical friction coefficient curves and (b) average friction coefficient and wear rate of the Co-Ni-P and Co-Ni-P/GO composite coatings.

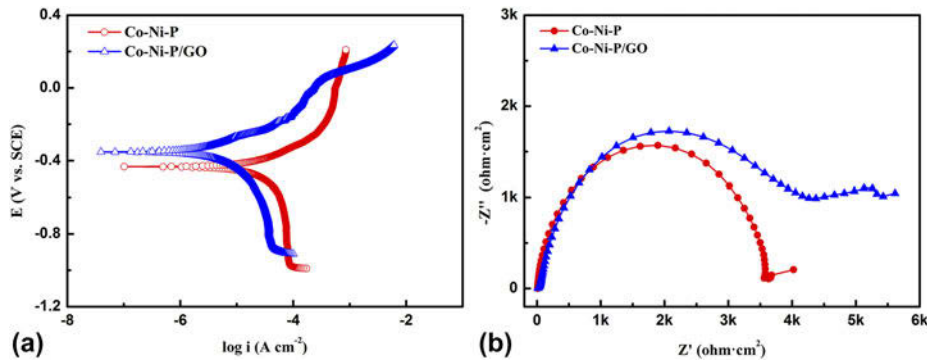


Figure 5: (a) Potentiodynamic polarization curves and (b) the Nyquist plots of the Co-Ni-P and Co-Ni-P/GO composite coatings measured in 3.5 wt% NaCl solution.

TABLE I: Corrosion potential (E_{corr}), corrosion current density (i_{corr}), and corrosion rate of Co-Ni-P and Co-Ni-P/GO composite coatings measured in 3.5 wt% NaCl solution.

Sample	E_{corr} (mV)	i_{corr} (A/cm ²)	Corrosion rate (mm/y)
Co-Ni-P	-433.7	14.33×10^{-6}	16.60×10^{-2}
Co-Ni-P/GO	-352.5	3.05×10^{-6}	3.54×10^{-2}

corrosion-resistant composite coating [26] and the conventional electroplated hard Cr coating [30].

The corrosion behavior of the Co-Ni-P and Co-Ni-P/GO composite coatings also measured by the powerful electrochemical technique, electrochemical impedance spectroscopy (EIS). Figure 5(b) shows the Nyquist plots of the coatings tested in 3.5 wt% NaCl solution. The diameter of the capacitive loop in the Nyquist plots reflects the polarization resistance of the coatings. As depicted in Fig. 5(b), the Co-Ni-P/GO composite coating has a larger diameter of the Nyquist loop than the Co-Ni-P coating. In other words, the Nyquist plot results further confirm that the Co-Ni-P/GO composite coating possesses better corrosion resistance immersed in 3.5 wt% NaCl solution than the Co-Ni-P coating.

Discussion

Hardness and wear mechanisms

As shown in Fig. 3, the Co-Ni-P/GO composite coatings display a higher microhardness of about 600 HV than the

Co-Ni-P coatings (450 HV). The improved microhardness is mainly attributed to the introduction of GO sheets into the Co-Ni-P matrix. On the one hand, the co-deposition of GO sheets promotes the capacity of the composite coating to prevent local deformation. GO sheets act as the reinforcements, blocking the dislocation motion during deformation process. On the other hand, GO sheets with good mechanical property also lead to the microhardness enhancement for the composite coatings. Thus, the microhardness of the composite coatings is improved significantly.

Figure 4 shows that the Co-Ni-P/GO composite coatings exhibit lower average COF and wear rate than the Co-Ni-P coatings. The remarkable anti-wear and friction-reducing performances of the Co-Ni-P/GO composite coatings are mainly caused by the following reasons. The introduction and uniformly distribution of the self-lubricating materials of GO sheets in the composite coatings cause the reduction of COF. Moreover, the co-deposition of superior mechanical GO sheets endows the Co-Ni-P/GO composite coatings with higher microhardness (Fig. 3). In terms of the classical Archard's law, the wear rate is inversely proportional to the microhardness, and thus, the Co-Ni-P/GO composite coatings obtain a lower wear rate.

Worn surface morphologies of the Co-Ni-P and Co-Ni-P/GO composite coatings sliding against GCr15 steel ball are given in

Fig. 6. It is clearly seen that there is a continuous wear scar on the worn surface of Co–Ni–P coating [Fig. 6(a)]. Besides, signs of adhesion, wear grooves along the sliding direction, and plastic deformation are also noted from its enlarged SEM image [Fig. 6(b)]. It can be concluded from these results that severe adhesive wear appeared during the sliding process, and the severe adhesive wear leads to the plastic deformation and then the wear loss of the Co–Ni–P coating is increased. Compared with Co–Ni–P coating, the Co–Ni–P/GO composite coating shows a discontinuous wear scar, only local surface has experienced the scuffing and wear [Fig. 6(c)]. The amplified SEM image [Fig. 6(d)] reveals that worn surface of the Co–Ni–P/GO composite coating is characterized by slight plastic deformation, and a few shallow scratches are seen on the wear track surface, which indicates that the wear mechanisms have changed from the severe adhesive wear for the Co–Ni–P coating to the abrasive wear and slight adhesive wear for the Co–Ni–P/GO composite coating.

Worn surface morphologies of the counterpart balls sliding against the Co–Ni–P and Co–Ni–P/GO composite coatings are depicted in Fig. 7. Oval wear scar and accumulation of wear debris are clearly visible on the counterpart steel ball sliding against Co–Ni–P coating, as shown in Fig. 7(a). The result suggests that severe adhesion wear occurred on this counterpart ball. The enlarged image of Fig. 7(b) shows obvious sign of delamination and cracks on the worn surface of this counterpart ball, which is because of the low microhardness of the Co–Ni–P coating. The high friction stress can give rise to

delamination of this coating and make it easier transfer to the counterpart steel ball. In contrast, Fig. 7(c) shows that the counterpart ball sliding against Co–Ni–P/GO composite coating displays an oval wear scar with smaller size and less accumulated wear debris on its surface than that counterpart ball of Co–Ni–P coating. However, delamination and small cracks are also observed on the magnified SEM image of the counterpart ball [Fig. 7(d)], which is because of the higher microhardness of the GCr15 (700 HV) than that of the Co–Ni–P/GO composite coatings (600 HV).

Electrochemical behavior

As depicted in Fig. 5, the Co–Ni–P/GO composite coating possesses better corrosion resistance immersed in 3.5 wt% NaCl solution than the Co–Ni–P coating. The incorporation of GO sheets is mainly responsible for the superior corrosion behavior of the Co–Ni–P/GO composite coating. For the Co–Ni alloy coating, when the coating is in contact with the corrosive medium (3.5 wt% NaCl), as a kind of strong adsorption anion, Cl^- tends to preferentially absorb on the defect of the coating. Soluble CoCl_2 and NiCl_2 are formed after the reaction of Cl^- with the Co^{2+} or Ni^{2+} . Then, the coating is corroded and more defects will appear on the corroded coating with the dissolution of CoCl_2 and NiCl_2 . The occurrence of more defects and dissolution of coating promote each other and speed up the infiltration of corrosive medium and the corrosion of the coating. For the Co–Ni–P/GO composite coating, the voids and cracks of the resulting composite

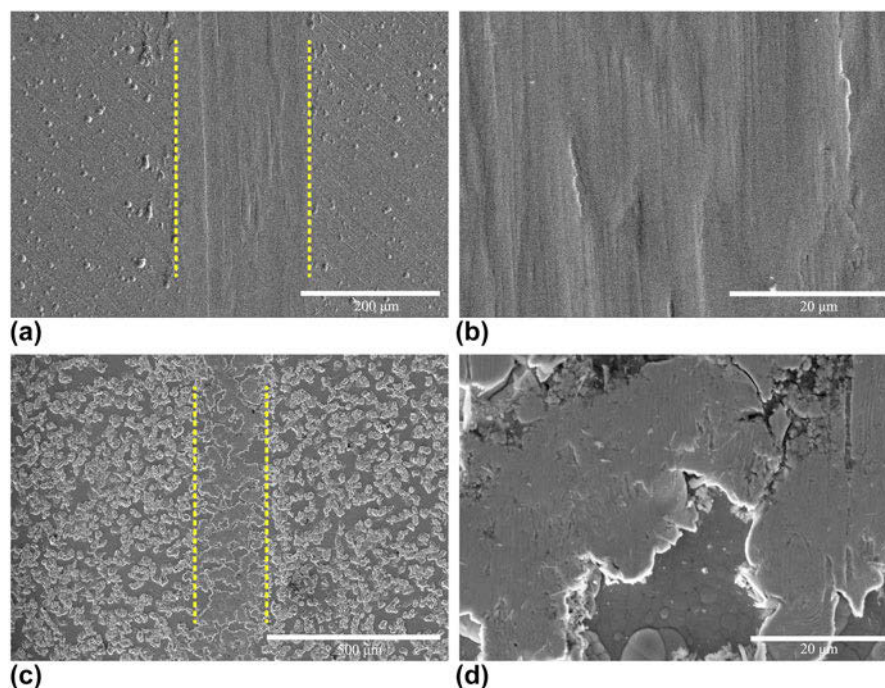


Figure 6: SEM morphologies of wear scars of the (a, b) Co–Ni–P and (c, d) Co–Ni–P/GO composite coatings.

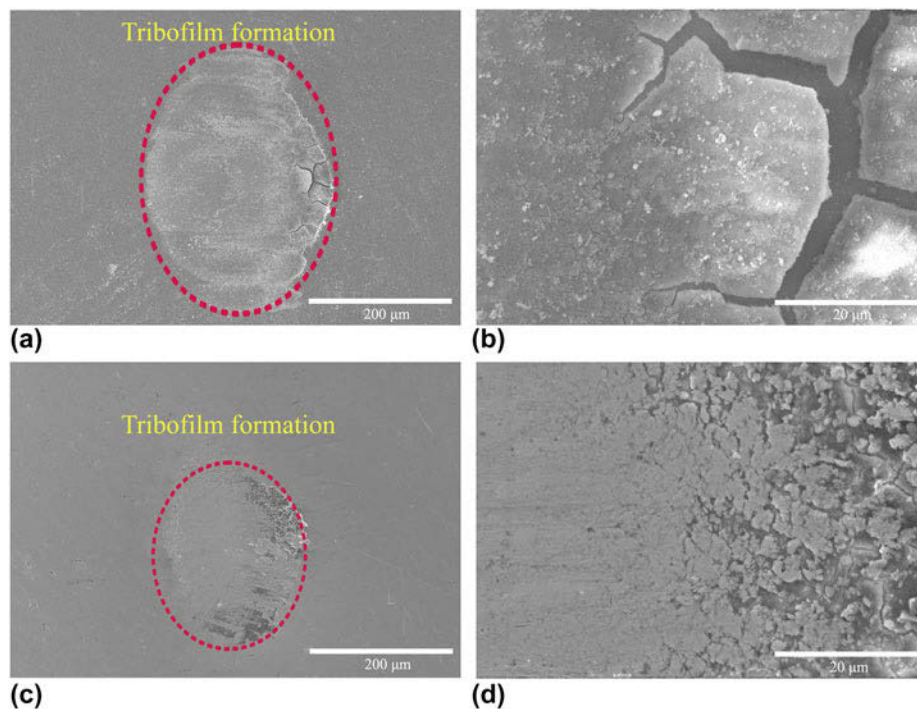


Figure 7: SEM morphologies of counterpart balls after sliding test against the (a, b) Co-Ni-P and (c, d) Co-Ni-P/GO composite coatings.

coating are filled by the embedded and uniform distributed GO sheets, which efficiently reduce the defects, the adsorption of corrosive anion (Cl^-), and the corrosion of the composite coating [31]. Besides, the corrosion channel is severely distorted by the embedded GO sheets in the Co-Ni-P matrix, the corrosive medium is obstructed from penetrating into the interface of coating and substrate, which makes stronger resistance to corrosion [32]. For the above reasons, the Co-Ni-P/GO composite coating shows a lower i_{corr} and corrosion rate and higher impedance value, i.e., superior anticorrosion capacity in the 3.5 wt% NaCl corrosive medium.

Conclusions

Co-Ni-P/GO composite coating was successfully fabricated by a pulse electrodeposition method. The co-deposition of GO sheets in the composite coatings is confirmed by SEM and Raman spectrum analysis. Morphologies, microhardness, and tribological and electrochemical performances of the Co-Ni-P/GO composite coatings are significantly affected by the embedded GO sheets. The Co-Ni-P/GO composite coating displays a rougher morphology, higher microhardness accompanied with more stability, and lower average COF during the sliding test against GCr15 steel balls, as well as lower corrosion rate in the electrochemical corrosion test carried out in 3.5 wt% NaCl solution. The improvement in friction reduction and anti-wear properties is attributed to embedded GO sheets, increasing the microhardness and the self-lubricating

performances of the Co-Ni-P/GO composite coating. Besides, the embedded GO sheets in the Co-Ni-P matrix can also serve as a suitable barrier and makes the permeation path more complex, prohibiting the corrosive medium from reaching the interface of coating and substrate, resulting in the superior corrosion resistance of the composite coating.

Experimental

Preparation of Co-Ni-P/GO composite coatings

An Intelligent Multiwave Electroplating Equipment (SMD-30P; Dashun Electroplating Equipment, Handan, China) was used for the power supply. The coatings were cathodically deposited on the 45 steel using a pulse current electrodeposition process. The bath compositions and electrodeposition parameters are given in Table II. The GO sheets were synthesized according to our previous reports. The number of GO layer was less than 10 layers, which was well characterized by transmission electron microscope and atomic force microscope in our previous works [33, 34]. The back of the substrate was covered by insulating tapes with an area of 5 cm^2 exposed in the electrolyte. Before the plating process, the surface of the 45 steel plates are mechanically polished with silicon carbide paper from 600 to 1500 P and then sequentially sonicated in acetone to remove oil contamination. After deposition, the specimens were taken out from the electrolyte, then rinsed with de-ionized water and dried immediately.

TABLE II: Bath compositions and the operational parameters for Co–Ni–P/GO composite coating electrodeposition.

Component/deposition condition	Concentration/value
Cobalt sulfate	50 g/L
Nickel sulfate	50 g/L
Sodium hypophosphite	10 g/L
Boric acid	40 g/L
Sodium citrate	40 g/L
Graphene oxide	0.2 g/L
pH	3.0
Temperature	45 °C
Current density	2.0 A/dm ²
Agitating speed	400 rpm
Deposition time	70 min
Duty cycle	20%
Anode: pure Ni plate	25 × 40 × 1 mm
Cathode: 45 steel	25 × 35 × 2 mm
Distance between anode and cathode	20 mm

Characterizations of the Co–Ni–P/GO coatings

Morphologies of the deposits were observed using SEM (SU8010, Hitachi, Tokyo, Japan). The element compositions were analyzed by EDS microanalyzer attached to the SEM and Raman microscope (Raman, LabRAM HR800, Horiba, Japan). The crystal structures of the coatings were characterized by XRD. The microhardness was measured with an Akashi MVK-H3 Vickers hardness tester, with a load of 25 g applied for 10 s. The average value from eight replicates for each kind of specimen was reported.

The friction and wear behaviors of the deposits were evaluated with a ball-on-disk tribometer (WTM-2E; Zhongke Kaihua Technology Development, Lanzhou, China). The tests were performed in air at room temperature and ambient humidity. GCr15 steel ball with diameter of 6.0 mm was used as the counterpart. The applied load is 2.0 N under the sliding speed of 200 rpm with a rotating radius of 4 mm. The duration of wear tests was 15 min. After the wear tests, the wear tracks were measured using a 3D laser measuring microscope (OLS4000; Olympus, Tokyo, Japan) to achieve the wear volume. The wear rates of all the films were calculated from $K = V/S \cdot F$, where V is the wear volume (mm³); S , the total sliding distance (m); and F , the normal load (N). Three replicate friction and wear tests were carried out for each specimen and the average value was reported with their errors. After sliding, the worn surfaces of the films and their corresponding counterpart balls were analyzed using the SEM.

A traditional three-electrode cell was established using the as-fabricated coatings as the working electrode, and a platinum plate and saturated calomel electrode as the counter and reference electrodes, respectively. Measurements were performed by an electrochemical workstation (CHI660E; Chenhua Instrument, Shanghai, China) at room temperature with 3.5 wt% NaCl solution as corrosive medium. Before

electrochemical tests, the samples were embedded in epoxy resin with an area of 1 cm² exposed to the corrosive medium. To obtain a stabilized system, all samples were immersed for 30 min before the potentiodynamic polarization and EIS tests. The potentiodynamic polarization curves were measured at a sweep rate of 1 mV/s from –300 to 300 mV versus the open circuit potential. EIS tests were studied in the frequency range from 10⁵ to 10^{–2} Hz utilizing a sinusoidal signal with 5 mV amplitude.

Acknowledgments

The authors are grateful to the financial support of the National Natural Science Foundation of China (51805089).

References

1. M. Leimbach, C. Tschaar, U. Schmidt, and A. Bund: Electrochemical characterization of chromium deposition from trivalent solutions for decorative applications by EQCM and near-surface pH measurements. *Electrochim. Acta* **270**, 104 (2018).
2. T.R. Tamilarasan, U. Sanjith, M.S. Shankar, and G. Rajagopal: Effect of reduced graphene oxide (rGO) on corrosion and erosion-corrosion behaviour of electroless Ni–P coatings. *Wear* **390**, 385 (2017).
3. A. Sadeghzadeh-Attar, G. AyubiKia, and M. Ehteshamzadeh: Improvement in tribological behavior of novel sol-enhanced electroless Ni–P–SiO₂ nanocomposite coatings. *Surf. Coat. Technol.* **307**, 837 (2016).
4. L. Wang, Y. Gao, Q. Xue, H. Liu, and T. Xu: A novel electrodeposited Ni–P gradient deposit for replacement of conventional hard chromium. *Surf. Coat. Technol.* **200**, 3719 (2006).
5. J. Wang, F.L. Zhang, T. Zhang, W.G. Liu, W.X. Li, and Y.M. Zhou: Preparation of Ni–P–diamond coatings with dry friction characteristics and abrasive wear resistance. *Int. J. Refract. Met. Hard Mater.* **70**, 32 (2017).
6. L. Wang, Y. Gao, Q. Xue, H. Liu, and T. Xu: Microstructure and tribological properties of electrodeposited Ni–Co alloy deposits. *Appl. Surf. Sci.* **242**, 326 (2005).
7. R. Jain and R. Pitchumani: Facile fabrication of durable copper based superhydrophobic surfaces via electrodeposition. *Langmuir* **34**, 3159 (2017).
8. A. Nicolenco, N. Tsyntsaru, J. Fornell, E. Pellicer, J. Reklaitis, D. Baltrunas, H. Cesiulis, and J. Sort: Mapping of magnetic and mechanical properties of Fe–W alloys electrodeposited from Fe(III)-based glycolate-citrate bath. *Mater. Des.* **139**, 429 (2018).
9. E. Beltowska-Lehman, P. Indyka, A. Bigos, M.J. Szczerba, J. Guspil, H. Koscielny, and M. Kot: Effect of current density on properties of Ni–W nanocomposite coatings reinforced with zirconia particles. *Mater. Chem. Phys.* **173**, 524 (2016).
10. A.M. Fernandez, J.A. Turner, B. Lara-Lara, and T.G. Deutsch: Preparation and characterization of Cu–Ga–Se thin films

- synthesized by electrodeposition: Effect of complexing agent and supporting electrolyte. *Mater. Chem. Phys.* **213**, 324 (2018).
11. **M. Najafi, A.A. Rafati, M.K. Fart, and A. Zare:** Effect of the pH and electrodeposition frequency on magnetic properties of binary $\text{Co}_{1-x}\text{Sn}_x$ nanowire arrays. *J. Mater. Res.* **29**, 190 (2014).
 12. **D.Y. Park, N.V. Myung, M. Schwartz, and K. Nobe:** Nanostructured magnetic CoNiP electrodeposits: Structure–property relationships. *Electrochim. Acta* **47**, 2893 (2003).
 13. **H. Wang, L. Wan, J. Zhang, Y. Chen, W. Hu, L. Liu, C. Zhong, and Y. Deng:** Enhanced microwave absorbing properties of surface-modified Co–Ni–P nanotubes. *Mater. Lett.* **169**, 193 (2016).
 14. **M. Rakap, E.E. Kalu, and S. Özkar:** Hydrogen generation from the hydrolysis of ammonia borane using cobalt–nickel–phosphorus (Co–Ni–P) catalyst supported on Pd-activated TiO_2 by electroless deposition. *Int. J. Hydrogen Energy* **36**, 254 (2011).
 15. **S. Mirzamohammadi, H. Khorsand, M. Aliofkhaezai, and D.V. Shtansky:** Effect of carbamide concentration on electrodeposition and tribological properties of Al_2O_3 nanoparticle reinforced nickel nanocomposite coatings. *Tribol. Int.* **117**, 68 (2017).
 16. **T. He, Y. He, H. Li, Y. Fan, Q. Yang, and Z. He:** A comparative study of effect of mechanical and ultrasound agitation on the properties of pulse electrodeposited Ni–W/MWCNTs composite coatings. *J. Alloys Compd.* **743**, 63 (2018).
 17. **M. Zhou, Y. Mai, H. Ling, F. Chen, W. Lian, and X. Jie:** Electrodeposition of CNTs/copper composite coatings with enhanced tribological performance from a low concentration CNTs colloidal solution. *Mater. Res. Bull.* **97**, 537 (2018).
 18. **S. Wang, S. Han, G. Xin, J. Lin, R. Wei, J. Lian, K. Sun, X. Zu, and Q. Yu:** High-quality graphene directly grown on Cu nanoparticles for Cu–graphene nanocomposites. *Mater. Des.* **139**, 181 (2018).
 19. **K. Stenberg, S. Dittrick, S. Bose, and A. Bandyopadhyay:** Influence of simultaneous addition of carbon nanotubes and calcium phosphate on wear resistance of 3D-printed Ti6Al4V. *J. Mater. Res.* **33**, 2077 (2018).
 20. **J. Wang, W. Wang, and J. Jia:** The oxidation resistance and tribological properties of Ni-based composites with in situ/ex situ Al_2O_3 and TiC ceramic phases at high temperatures. *J. Mater. Res.* **31**, 3262 (2016).
 21. **S. Qiu, G. Liu, W. Li, H. Zhao, and L. Wang:** Noncovalent exfoliation of graphene and its multifunctional composite coating with enhanced anticorrosion and tribological performance. *J. Alloys Compd.* **747**, 60 (2018).
 22. **M. Mirzaee, C. Dehghanian, and K.S. Bokati:** One-step electrodeposition of reduced graphene oxide on three-dimensional porous nano nickel–copper foam electrode and its use in supercapacitor. *J. Electroanal. Chem.* **813**, 152 (2018).
 23. **Y.J. Mai, M.P. Zhou, H.J. Ling, F.X. Chen, W.Q. Lian, and X. H. Jie:** Surfactant-free electrodeposition of reduced graphene oxide/copper composite coatings with enhanced wear resistance. *Appl. Surf. Sci.* **433**, 232 (2018).
 24. **C. Liu, F. Su, and J. Liang:** Producing cobalt–graphene composite coating by pulse electrodeposition with excellent wear and corrosion resistance. *Appl. Surf. Sci.* **351**, 889 (2015).
 25. **C.M.P. Kumar, T.V. Venkatesha, and R. Shabadi:** Preparation and corrosion behavior of Ni and Ni–graphene composite coatings. *Mater. Res. Bull.* **48**, 1477 (2013).
 26. **J. Jiang, C. Feng, W. Qian, L. Zhu, S. Han, and H. Lin:** Effect of graphene oxide nanosheets and ultrasonic electrodeposition technique on Ni–Mo/graphene oxide composite coatings. *Mater. Chem. Phys.* **199**, 239 (2017).
 27. **Z. Xue, W. Lei, Y. Wang, H. Qian, and Q. Li:** Effect of pulse duty cycle on mechanical properties and microstructure of nickel–graphene composite coating produced by pulse electrodeposition under supercritical carbon dioxide. *Surf. Coat. Technol.* **325**, 417 (2017).
 28. **Q. Zhang, Z. Qin, Q. Luo, Z. Wu, L. Liu, B. Shen, and W. Hu:** Microstructure and nanoindentation behavior of Cu composites reinforced with graphene nanoplatelets by electroless co-deposition technique. *Sci. Rep.* **7**, 1338 (2017).
 29. **T.S.N. Sankara Narayanan, I. Baskaran, K. Krishnaveni, and S. Parthiban:** Deposition of electroless Ni–P graded coatings and evaluation of their corrosion resistance. *Surf. Coat. Technol.* **200**, 3438 (2006).
 30. **L. Qiao, Y. Wu, S. Hong, Y. Qin, W. Shi, and G. Li:** Corrosion behavior of HVOF-sprayed Fe-based alloy coating in various solutions. *J. Mater. Eng. Perform.* **26**, 3813 (2017).
 31. **A.A. Aal, S.M. El-Sheikh, and Y.M.Z. Ahmed:** Electrodeposited composite coating of Ni–W–P with nano-sized rod- and spherical-shaped SiC particles. *Mater. Res. Bull.* **44**, 151 (2009).
 32. **N.S. Qu, D. Zhu, and K.C. Chan:** Fabrication of Ni– CeO_2 nanocomposite by electrodeposition. *Scr. Mater.* **54**, 1421 (2006).
 33. **Y.J. Mai, J.P. Tu, C.D. Gu, and X.L. Wang:** Graphene anchored with nickel nanoparticles as a high-performance anode material for lithium ion batteries. *J. Power Sources* **209**, 1 (2012).
 34. **Y.J. Mai, X.L. Wang, J.Y. Xiang, Y.Q. Qiao, D. Zhang, C.D. Gu, and J.P. Tu:** CuO/graphene composite as anode materials for lithium-ion batteries. *Electrochim. Acta* **56**, 2306 (2011).